J Sign Process Syst
DOI 10.1007/s11265-014-0933-9

High Frame Rate 3-D Ultrasound Imaging Using Separable Beamforming

Ming Yang · Richard Sampson · Siyuan Wei · Thomas F. Wenisch · Chaitali Chakrabarti

Received: 20 February 2014 / Accepted: 17 July 2014

Abstract Recently, there has been great interest in 3-D ultrasound imaging, but power constraints have precluded practical implementation of high-resolution and high-frame-rate 3-D ultrasound in handheld imaging platforms. In this paper, we propose a separable beamforming procedure for both 3-D synthetic aperture and plane wave systems that drastically reduces computational and hence power requirements. Separable beamforming approximates 2-D array beamforming for 3-D images through a series of beamforming operations on 1-D arrays. Our proposed method is based on a separable delay decomposition method that minimizes phase error. We show that the proposed separable synthetic aperture system achieves 19-fold complexity reduction and the proposed plane wave separable system achieves 12-fold complexity reduction compared to the corresponding non-separable beamforming baseline systems. Furthermore, we verify the performance of the fixed-point-precision separable beamforming and iterative delay calculation through Field II simulations. Our results show that both the synthetic aperture system and the plane wave system can produce images with the same quality as images generated by non-separable beamforming. We also briefly describe how the two types of separable beamformer can be implemented on a modified version of Sonic Millip3De, our recently proposed hardware accelerator for the digital front-end of a 3-D ultrasound system.

Keywords Separable beamforming · Separable delay · Synthetic aperture · Plane wave · 2-D array · Hardware implementation

M. Yang (✉) · S. Wei · C. Chakrabarti
School of Electrical, Computer and Energy Engineering, Arizona State University, Tempe, AZ 85287, USA
e-mail: m.yang@asu.edu

S. Wei
e-mail: siyuan.wei@asu.edu

C. Chakrabarti
e-mail: chaitali@asu.edu

R. Sampson · T. F. Wenisch
Department of Electrical Engineering and Computer Science, University of Michigan, Ann Arbor, MI 48109, USA
e-mail: rsamp@umich.edu

T. F. Wenisch
e-mail: twenisch@umich.edu

1 Introduction

Ultrasound imaging is one of the most popular medical imaging modalities; it is inexpensive relative to CT and MRI and poses no known side-effects. Unlike other imaging modalities, generating and sensing ultrasound signals does not require high power, which makes handheld ultrasound imaging systems feasible.

Recently, there has been a great deal of interest in development of 3-D ultrasound imaging systems, which generate volumetric images that are easier to interpret and lead to better diagnosis [2, 16]. In this paper, we study two popular 3-D ultrasound imaging techniques: Synthetic Aperture Ultrasound (SAU) imaging and plane wave imaging. In a SAU system, a high resolution image is synthesized from multiple low resolution images obtained from multiple sub-apertures[7, 10]. Thus, SAU systems are good for high resolution 3-D B-mode imaging application. These systems can only support low to medium frame rates due to their high computational complexity. In contrast, plane wave systems offer extremely high frame rates at the cost of reduced SNR and reduced resolution compared to conventional

Published online: 22 August 2014

phased array systems. In a plane wave system, hundreds of parallel scanlines can be generated in each firing. Thus, these systems can support the high frame rates required by applications in 3-D flow imaging and 3-D elastography.

Implementing a high-resolution, high-image-quality, and high-frame-rate 3-D ultrasound system within the power budget constraints of a handheld device is even more challenging, and no commercial offerings of hand-held 3-D ultrasound yet exist. We recently proposed Sonic Millip3De [14], a 3-D die-stacking hardware accelerator for ultrasound beamforming, which enables a SAU-based system to generate a 3-D volume with 45° in both azimuth and elevation view angles and 10cm maximum depth at 1 frame/second within a 16W system power budget in 45nm technology. Sonic Millip3De leverages subaperture processing [9, 12] and a narrow-bit-width streaming hardware architecture that eliminates much of the computational complexity of delay calculation. More recently, we proposed an optimized subaperture apodization and firing scheme, which reduces the number of firings by half and hence the system power consumption [15]. Nevertheless, the existing design still falls short of desirable power targets (e.g., 5W for safe contact with human skin), calling for further reductions in front-end processing requirements. Processing might be further reduced by utilizing sparse 2-D arrays [3, 11], but at significant cost in image quality due to artifacts from grating lobes and larger sidelobes.

An alternative approach to reduce front-end complexity is to use separable beamforming [5, 13], wherein conventional 2-D array beamforming is decomposed into a series of 1-D beamforming processes at the cost of some reduction in image quality. A frequency-domain separable beamforming method was proposed in [5] that is amenable to parallel execution but can not support dynamic focusing, and has lower image quality. An X-Y separable beamforming for systems with rectangular scan geometry (scanlines are perpendicular to the 2-D array plane) was proposed in [13]. However this method is applicable only to rectangular scan systems.

In our previous work [17], we proposed a new separable beamforming delay decomposition method for SAU systems that was not restricted to any specific scan system. It was based on a delay decomposition method that minimizes the root-mean-square (RMS) phase error introduced by the separable delay approximation.

In this paper, we extend our method to plane wave systems. We show that the proposed delay decomposition is quite simple and yet it significantly reduces phase error compared to the method proposed in [13]. We also modify the original Sonic Millipe3De architecture to implement the separable beamforming algorithm efficiently for both SAU and plane wave systems. Finally, we show that, for both systems, the proposed separable algorithm produces 3-D images with high quality that is almost the same as non-separable baselines. Furthermore, images produced with 12-bit-fixed-point precision are comparable in quality to those generated using double-precision-floating-point arithmetic.

The remainder of this paper is organized as follows. In Section 2, we provide background on SAU and plane wave imaging techniques. In Section 3, we present the separable beamforming method and RMS-delay-minimizing decomposition method for both SAU and plane wave systems. In Section 4, we present the changes required by separable beamforming algorithm for the Sonic Millipe3De architecture. Simulation results are shown in Section 5. Section 6 concludes the paper.

2 Background

2.1 Subaperture-based SAU System

Synthetic aperture imaging (SAU) is a popular imaging mode that has been used in ultrasound systems for the past few decades. It can support high frame rates compared to phased array imaging, since its frame rate does not depend on the number of scanlines. It also enables better resolution, since its beamforming is equivalent to performing both transmit and receive dynamic focusing [7, 10]. In a classic synthetic aperture ultrasound imaging system, in each transmission, only one transducer element transmits and all elements receive. After each transmit, a low resolution image is formed. Multiple low resolution images are combined to obtain a high resolution image.

However, the classic SAU system suffers from low SNR because only one transducer fires at a time [7], and requires many more concurrent channels in a 3-D system. To address these problems, we proposed a firing method based on overlapping subapertures where each virtual source corresponds to a subaperture. Our approach is a generalization of the 1-D sub-aperture scheme proposed in [9]. Virtual source firing improves SNR and subaperture receive reduces the number of concurrent channels.

In this work, we employ a similar firing scheme to enable high frame rates. As shown in Fig. 1, each subaperture has 32×32 elements and neighboring subapertures overlap by 24×32 elements. Each virtual source is implemented by 76 transducers located in the center of the corresponding subaperture and fires only once. After each firing, both the virtual source and the receive subaperture shift by 8 elements to an adjacent location. This scheme requires 96 firings.

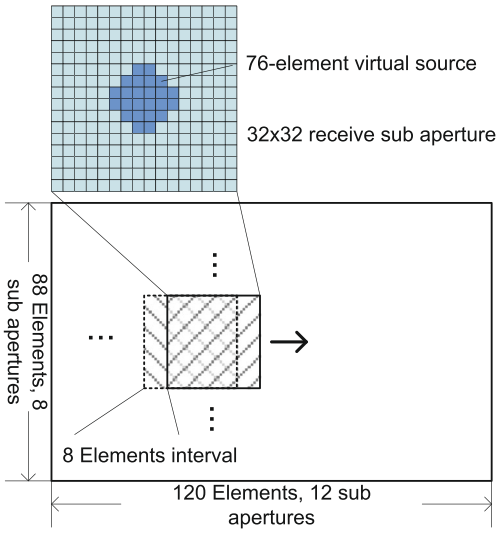

Figure 1 Overlapped subaperture processing in SAU system.

2.2 Plane Wave System

The transmit and receive scheme of a plane wave system is shown in Fig. 2. We assume that only a subset of transducers in the physical aperture is used for plane wave imaging. This subset is referred to as the receive aperture; its location is fixed. In each firing, the receive aperture is used to generate a plane wave that propagates through the region of interest. All the elements on this receive aperture are used to receive echo signals. Within the receive aperture, subsets of elements form a sequence of beamforming apertures (one such aperture is shown by a bold box in Fig. 2), which traverse all possible positions within the receive aperture. In each position, the beamforming aperture generates a single vertical scanline located at its center. When part of the beamforming aperture is outside the receive aperture, the corresponding signals are assumed to be zero. If the receive aperture is of size $K \times K$, the beamforming generates $K \times K$ scanlines. In general, the transmit and receive scheme of plane wave systems allows several hundred scanlines to be generated per transmit, thus greatly increasing the peak frame rate.

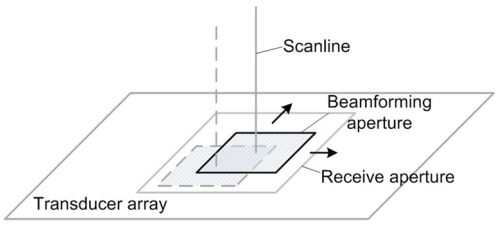

Figure 2 2-D Plane Wave Transmit and Receive Scheme.

3 Separable Beamforming

3.1 Motivation

Consider a 3-D SAU system described by the configuration shown in Table 1. To generate a 3-D image of size 10cm $\times$ 45° $\times$ 45°, 1.1×10^{12} delay-sum operations must be performed per frame. Such high computational complexity results in correspondingly high power consumption and thus limits hand-held applications of 3-D ultrasound.

Separable beamforming can significantly reduce computational complexity by decomposing 2-D array beamforming into two stages of 1-D beamforming. In the first stage, the beamsums are computed along one direction (e.g., horizontal), and in the second stage the beamsums are computed along the other direction (e.g., vertical).

3.2 Separable Beamforming Process

Without loss of generality, we assume the 3-D coordinate system shown in Fig. 3. Let (R, θ, ϕ) be the coordinates of a focal point P. Here R is the radial distance from the origin O to point P. Point P' is the orthogonal projection of P in the yz plane. ϕ is the elevation angle between line OP' and the z axis. θ is the azimuth angle between OP and its orthogonal projection OP' in the yz plane. For a transducer array element at $(x, y, 0)$, the distance between the transducer element and the focal point P is given by

$$d = \sqrt{R^2 + x^2 - 2Rx\sin(\theta) + y^2 - 2Ry\cos(\theta)\sin(\phi)} \quad (1)$$

Table 1 System parameters of the 3-D SAU system.

Property	Value
Pitch, μm	192.5
Array size, element	120 $\times$ 88
Subaperture size, element	32 $\times$ 32
Number of scanlines	48 $\times$ 48
View angle, square degree	45° $\times$ 45°
Max depth, cm	10
Center frequency, MHz	4
6dB transducer bandwidth, MHz	2
A/D sampling rate, MHz	40

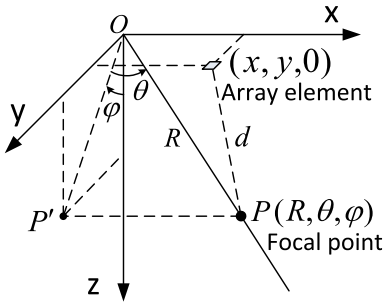

Figure 3 Array and beamforming coordinate system.

Assuming that the ultrasound speed is c, and the round-trip delay between the origin and the focal point is $2R/c$, the round-trip delay at the transducer relative to that at the origin is given by

$$\tau(x, y, R, \theta, \phi) = (2R - d_{\text{transmit}} - d_{\text{receive}})/c \tag{2}$$

Let $\tau(n_x, n_y, m_R, m_\theta, m_\phi)$ be the discrete form of $\tau(x, y, R, \theta, \phi)$, where n_x and n_y are variables associated with the coordinates of receive elements, and m_R, m_θ and m_ϕ are variables associated with the coordinates of focal points. Then the non-separable beamforming corresponding to subaperture l of size $N_x \times N_y$ whose left corner indices are i_l and j_l, is described as

$$F_l(m_R, m_\theta, m_\phi; t) = \sum_{n_x=i_l}^{i_l+N_x-1} \sum_{n_y=j_l}^{j_l+N_y-1} A_l(n_x, n_y) \cdot S_l(n_x, n_y, t - \tau(n_x, n_y, m_R, m_\theta, m_\phi))$$

where $S_l(n_x, n_y, t)$ is the signal received by transducer element (n_x, n_y) at lth firing and $A_l(n_x, n_y)$ is the corresponding apodization coefficient. $F_l(m_R, m_\theta, m_\phi; t)$ is the low resolution 3-D image generated by subaperture l. F_l should be sampled at $t = 2R/c$ for dynamic focusing. For a synthetic aperture ultrasound system, the final high resolution image is obtained by summing all the low resolution images from all subapertures.

Now, if $\tau(n_x, n_y, m_R, m_\theta, m_\phi)$ can be decomposed as

$$\tau(n_x, n_y, m_R, m_\theta, m_\phi) = \tau_1(n_x, n_y, m_R, m_\theta) + \tau_2(n_y, m_R, m_\theta, m_\phi) \tag{3}$$

then Eq. 3 can be represented by a two-stage separable beamforming process:

$$F_l^{(1)}(n_y, m_R, m_\theta; t) = \sum_{n_x=i_l}^{i_l+N_x-1} A_l(n_x, n_y) S_l(n_x, n_y, t - \tau_1(n_x, n_y, m_R, m_\theta)) \tag{4}$$

$$F_l^{(2)}(m_R, m_\theta, m_\phi; t) = \sum_{n_y=j_l}^{j_l+N_y-1} F_l^{(1)}(n_y, m_R, m_\theta; t - \tau_2(n_y, m_R, m_\theta, m_\phi)) \tag{5}$$

In the first stage, beamforming is done along the x axis, which functions as a spatial filter that steers the receive plane to azimuth angle θ. The process repeats for all combinations of m_R, n_y and m_θ and results in a partially beamformed intermediate signal $F_l^{(1)}$. In the second stage, 1-D beamforming is performed along the y axis, and corresponds to steering receive plane to elevation angle ϕ. The second stage beamforming is repeated for all combinations of m_R, m_θ and m_ϕ. The principle of the proposed separable beamforming method is shown in Fig. 4.

The number of delay-sum operations of separable beamforming for one subaperture is $N_x N_y M_R M_\theta + N_y M_R M_\theta M_\phi$ in contrast to $N_x N_y M_R M_\theta M_\phi$ in conventional, non-separable beamforming, where $N_x \times N_y$ is the size of a subaperture, M_R is the number of focal points on a scanline, and $M_\theta \times M_\phi$ is the number of scanlines. Thus, the computational complexity reduction is $N_x M_\phi/(N_x + M_\phi)$. For the configuration shown in Table 1 with a 32×32 subaperture size and 48×48 scanlines, our approach achieves about $19\times$ complexity reduction.

The separable beamforming method is based on the assumption that the wave propagation delay τ can be decomposed into τ_1 and τ_2. However the decomposition is not exact and its effectiveness depends on the accuracy of the τ_1 and τ_2 approximations. Next, we describe the

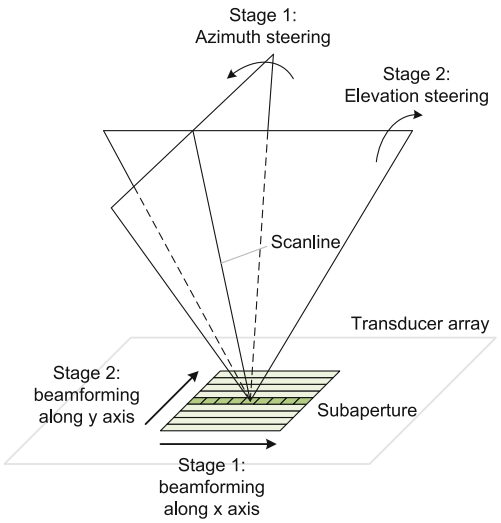

Figure 4 The principle of separable beamforming.

proposed decomposition method, which designs τ_1 and τ_2 to minimize RMS phase error.

3.3 Delay Decomposition For SAU System

The beamsum delay τ is a function of five variables x, y, R, θ, and ϕ. This function cannot be strictly decomposed into a sum of two functions with fewer variables because the distance calculation involves a square root operation (as shown in Eq. 1). The Taylor series of the square root includes cross terms, which can not be easily decomposed. To make the delay equation separable, some of these cross terms must be dropped. Although the effect of the cross terms diminish with large R, for shallow depths, the cross terms in the delay calculation can be significant.

Consider a simple delay decomposition that is given by $\tau(x, y, R, \theta, \phi) = \tau_1(x, R, \theta) + \tau_2(y, R, \phi)$, where both τ_1 and τ_2 are functions of three variables. For dynamic focusing, both τ_1 and τ_2 depend on R. τ_1 is also a function of θ and x because 1-D beamforming along x direction allows the array system to distinguish signals coming from different azimuth angles. Similarly, τ_2 is a function of y and ϕ since 1-D beamforming along y direction allows the array system to distinguish signals coming from different elevation angles. Unfortunately this simple decomposition has large errors primarily because θ and ϕ are separated and the cross term involving θ and ϕ is lost.

One way to solve this problem is by increasing the number of variables of τ_1 and τ_2. For τ_1, adding y to the variable list helps retain cross terms between x and y and thus should be considered. There is no benefit in adding ϕ to the variable list because 1-D beamforming in the first stage is along the x direction, and does not have enough resolution along ϕ. Similarly for τ_2, adding θ to the variable list has the benefit of preserving cross terms involving θ and ϕ. Adding x to τ_2 is not a good option because neither the input signal of second-stage beamforming $F^{(1)}$ nor output of second stage beamforming $F^{(2)}$ contains x. By increasing the number of variables of τ_1 and τ_2 from three variables to four, the approximation error is reduced by one decade.

Given this decomposition, we next generate $\tau_1(x, y, R, \theta)$ and $\tau_2(y, R, \theta, \phi)$ such that the error due to approximation is minimized. Minimizing RMS error is equivalent to minimizing

$$E(y, R, \theta) = \int_{\phi_1}^{\phi_2} \int_{x_1}^{x_2} [\tau(x, y, R, \theta, \phi) - (\tau_1(x, y, R, \theta) + \tau_2(y, R, \theta, \phi))]^2 dx d\phi \quad (6)$$

where x varies from x_1 to x_2 along the x direction of the subaperture, and ϕ varies between ϕ_1 and ϕ_2. This is a classic calculus of variation problem that can be solved by the Euler-Lagrange equation [4]. The discrete version of τ_1 and τ_2 that minimizes RMS error is given by

$$\tau_1(n_x, n_y, m_R, m_\theta) = \frac{1}{M_\phi} \sum_{m_\phi=1}^{M_\phi} \tau(n_x, n_y, m_R, m_\theta, m_\phi) - \rho(n_y, m_R, m_\theta) \quad (7)$$

$$\tau_2(n_y, m_R, m_\theta, m_\phi) = \frac{1}{N_x} \sum_{n_x=i_l}^{i_l+N_x-1} \tau(n_x, n_y, m_R, m_\theta, m_\phi) - \rho(n_y, m_R, m_\theta) \quad (8)$$

$$\rho(n_y, m_R, m_\theta) = \frac{1}{2N_x M_\phi} \sum_{n_x=i_l}^{i_l+N_x-1} \sum_{m_\phi=1}^{M_\phi} \tau(n_x, n_y, m_R, m_\theta, m_\phi) \quad (9)$$

Note that Eqs. 7 and 8 are not the only form that minimizes RMS error. Assuming we add an arbitrary term $\xi(n_y, m_R, m_\theta)$ on the right-hand side of Eq. 7 while subtracting it from the right-hand side of Eq. 8, the summation of τ_1 and τ_2 and the RMS error both remain the same. In this work, we choose $\xi(n_y, m_R, m_\theta) = 0$ so that the mean values of τ_1 and τ_2 are the same. From an architectural perspective, this formulation makes the delay line length or buffer depth roughly equal in the two beamforming stages.

3.4 Separable Beamforming For Plane Wave Systems

The scanline geometry in a plane wave system is shown in Fig. 5. In this system, the scanlines are all parallel to each other and perpendicular to the transducer plane, which means $\theta = 0$ and $\phi = 0$ for all scanlines. If $(x, y, 0)$ is the coordinate of a transducer element, and $(\hat{x}, \hat{y}, \hat{z})$ is the coordinate of focal point P, then the delay τ is the difference between the round trip delay at $(\hat{x}, \hat{y}, 0)$ and round trip delay at $(x, y, 0)$, namely $\tau = \frac{1}{c}[|\hat{z}| - \sqrt{(x-\hat{x})^2 + (y-\hat{y})^2 + \hat{z}^2}]$, where c is the speed of sound.

Similar to the SAU case, let (n_x, n_y) be the transducer index and $(m_{\hat{x}}, m_{\hat{y}}, m_{\hat{z}})$ be the focal point index. Assuming the receive signal at transducer (n_x, n_y) is $S(n_x, n_y, t)$, the non-separable beamforming for a plane wave system is given by

$$F(m_{\hat{x}}, m_{\hat{y}}, m_{\hat{z}}; t) = \sum_{n_x=m_{\hat{x}}-\frac{N_x}{2}}^{m_{\hat{x}}+\frac{N_x}{2}-1} \sum_{n_y=m_{\hat{y}}-\frac{N_y}{2}}^{m_{\hat{y}}+\frac{N_y}{2}-1} A(n_x - m_{\hat{x}}, n_y - m_{\hat{y}}) \cdot S(n_x, n_y, t - \tau(n_x - m_{\hat{x}}, n_y - m_{\hat{y}}, m_{\hat{z}})) \quad (10)$$

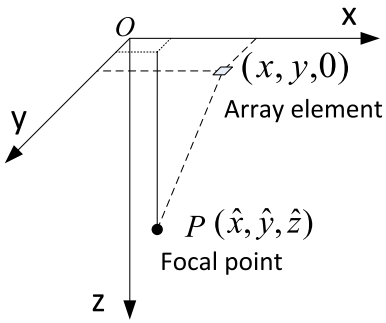

Figure 5 Scan geometry of plane wave system.

where N_x is the number of columns and N_y is number of rows of a beamforming aperture.

Let $\Delta n_x = n_x - m_{\hat{x}}$ and $\Delta n_y = n_y - m_{\hat{y}}$, we have

$$F(m_{\hat{x}}, m_{\hat{y}}, m_{\hat{z}}; t) = \sum_{\Delta n_x=-\frac{N_x}{2}}^{\frac{N_x}{2}-1} \sum_{\Delta n_y=-\frac{N_y}{2}}^{\frac{N_y}{2}-1} A(\Delta n_x, \Delta n_y) \cdot S(m_{\hat{x}} + \Delta n_x, m_{\hat{y}} + \Delta n_y, t - \tau(\Delta n_x, \Delta n_y, m_{\hat{z}})) \quad (11)$$

Because θ and ϕ are fixed in a plane wave system, delay decomposition is simpler than in a SAU system. The function τ can be decomposed as $\tau(\Delta n_x, \Delta n_y, m_{\hat{z}}) = \tau_1(\Delta n_x, m_{\hat{z}}) + \tau_2(\Delta n_y, m_{\hat{z}})$ since Δn_x and Δn_y are independent variables. Separable beamforming can then be represented as follows:

$$F^{(1)}(n_y, m_{\hat{x}}, m_{\hat{z}}; t) = \sum_{\Delta n_x=-\frac{N_x}{2}}^{\frac{N_x}{2}-1} A_x(\Delta n_x) \cdot S(m_{\hat{x}} + \Delta n_x, n_y, t - \tau_1(\Delta n_x, m_{\hat{z}})) \quad (12)$$

$$F^{(2)}(m_{\hat{x}}, m_{\hat{y}}, m_{\hat{z}}; t) = \sum_{\Delta n_y=-\frac{N_y}{2}}^{\frac{N_y}{2}-1} A_y(\Delta n_y) \cdot F^{(1)}(m_{\hat{y}} + \Delta n_y, m_{\hat{x}}, m_{\hat{z}}; t - \tau_2(\Delta n_y, m_{\hat{z}})) \quad (13)$$

Figure 6 demonstrates this process. In the first stage, beamforming is performed along the x dimension. The 1-D beamforming aperture traverses the entire receive aperture. On each combination of $(m_{\hat{x}}, n_y)$, a 1-D beamformer steers the azimuth angle to be normal to the xy plane, and records partially beamformed data in $F^{(1)}(n_y, m_{\hat{x}}, m_{\hat{z}}; t)$. As in non-separable beamforming, when the beamforming aperture is partially outside the receive aperture, the missing signals are assumed to be zero. The second-stage beamforming is done along the y dimension. The 1-D beamforming aperture moves along the y dimension and traverses the entire receive aperture. On each combination of $(m_{\hat{x}}, m_{\hat{y}})$, the beamformer steers the elevation angle to be normal to the xy plane and a scanline is generated. The computation complexity reduction of the separable method compared to the non-separable method is $N_x M_{\hat{y}}/(N_x + M_{\hat{y}})$, where N_x is number of transducers columns in a receive aperture in

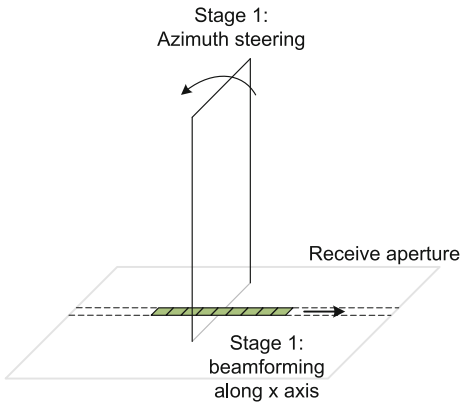

(a) Plane wave separable beamforming, stage 1

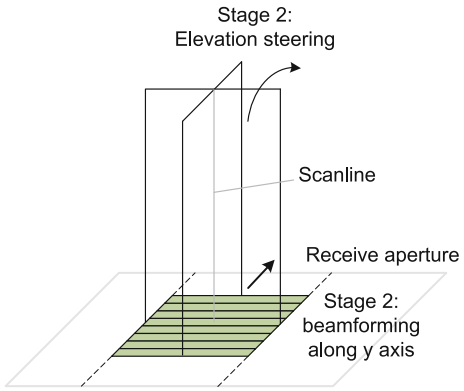

(b) Plane wave separable beamforming, stage 2

Figure 6 Plane wave separable beamforming principle.

the x dimension, and $M_{\hat{y}}$ is the number of scanlines in a 3D image in the y dimension. Thus separable beamforming in a plane wave system results in 12× reduction if the beamforming aperture size is 20×20, and the 3D volume has 32×32 scanlines.

As in the SAU system, here we minimize the RMS error for delay decomposition, which is equivalent to minimizing the error function by appropriate choice of τ_1 and τ_2.

$$E(\hat{z}) = \int_{-\frac{y_0}{2}}^{\frac{y_0}{2}} \int_{-\frac{x_0}{2}}^{\frac{x_0}{2}} [\tau(\Delta x, \Delta y, \hat{z}) - (\tau_1(\Delta x, \hat{z}) + \tau_2(\Delta y, \hat{z}))]^2 d\Delta x d\Delta y \quad (14)$$

The discrete version of a solution to this problem is given by:

$$\tau_1(\Delta n_x, m_{\hat{z}}) = \frac{1}{N_y} \sum_{\Delta n_y=-\frac{N_y}{2}}^{\frac{N_y}{2}-1} \tau(\Delta n_x, \Delta n_y, m_{\hat{z}}) - \rho(m_{\hat{z}}) \quad (15)$$

$$\tau_2(\Delta n_y, m_{\hat{z}}) = \frac{1}{N_x} \sum_{\Delta n_x=-\frac{N_x}{2}}^{\frac{N_x}{2}-1} \tau(\Delta n_x, \Delta n_y, m_{\hat{z}}) - \rho(m_{\hat{z}}) \quad (16)$$

$$\rho(m_{\hat{z}}) = \frac{1}{2N_xN_y} \sum_{\Delta n_y=-\frac{N_y}{2}}^{\frac{N_y}{2}-1} \sum_{\Delta n_x=-\frac{N_x}{2}}^{\frac{N_x}{2}} \tau(\Delta n_x, \Delta n_y, m_{\hat{z}}) \quad (17)$$

In Fig. 7, the RMS error of our proposed delay decomposition method is compared with that of Owen et al. [13]. The results indicate that our proposed method has lower phase error, and as depth increases the error rapidly reduces. However, as subaperture size increases, the error increases for both methods. We present Field II simulation results for both methods in Section 5.

3.5 Online Iterative Separable Delay Calculation

Next we focus on efficient calculation of τ_1 and τ_2. Eqs. 7 and 8 for SAU systems or Eqs. 15 and 16 for plane wave systems can be used to generate look-up tables. However, storing τ_1 and τ_2 as look-up tables is not practical due to the large look-up table size. Especially for our SAU system configuration, look-up tables of τ_1 and τ_2 for 96 subapertures include at least (even considering symmetry) 5.7 billion and 8.9 billion constants, respectively.

Fortunately, the delay values of consecutive samples on a scanline do not change much. Hence, it is possible to iteratively calculate the delay value for the ith focal point on a scanline from the delay value of the $(i-1)$th focal point. We use piece-wise quadratic curves to approximate the delay difference between consecutive samples along a scanline. For example, let $\tilde{\tau}(m_R)$ be the delay corresponding to the m_Rth focal point for fixed n_x and n_y. Let $\eta(m_R) = \tilde{\tau}(m_R+1) - \tilde{\tau}(m_R)$, then $\eta(m_R)$ can be approximated by $am_R^2 + bm_R + c$. Instead of storing the delay look-up table directly, the coefficients a, b and c and the initial delay are stored, and the delays are iteratively calculated using these coefficients. The iterative calculation method does not require multiplications; it can be implemented using only three additions. A similar iterative delay calculation was employed for non-separable beamforming in [14].

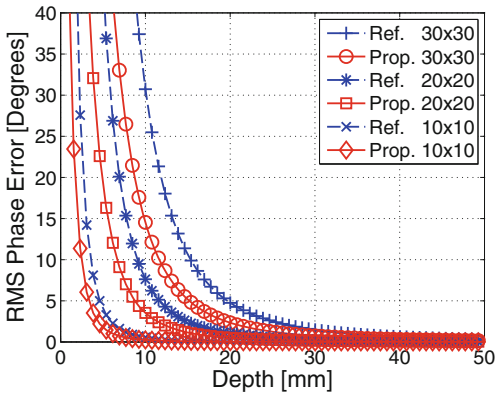

Figure 7 RMS phase error of proposed delay decomposition compared with the method in [13].

For the SAU system, each scanline is divided into 2-4 sections and the delays in each section are approximated by a quadratic curve. For our SAU system configuration we choose 3 sections, each characterized by three constants and an initial point, and each scanline requires an additional start index. Thus, each scanline requires 13 constants. A total of 38 million constants must be stored; 15 million constants are required for τ_1 and the remaining 23 million constants for τ_2. The 15 million constants for τ_1 correspond to 13 constants/scanline × 48 scanlines × 1,024 transducers/subaperture × 96 subapertures, divided by 4 due to symmetry. The number of constants for τ_2 is calculated in a similar way. Each constant requires 12 bits on average [15], resulting an overall storage requirement of 55MB.

For the plane wave system, the beamforming aperture size is 20×20. Each scanline is also divided into 3 sections with 13 constants per scanline. A total of 260 constants are required with 130 constants from each of τ_1 and τ_2. The 130 constants correspond to 13 constants/scanline × 1 scanline/channel × 20 channels, divided by 2 due to symmetry. Each constant requires 12 bits on average, resulting in an overall storage requirement of only 390B for the plane wave system.

Figures 8 and 9 shows simulation results of the iterative delay calculation method with double-precision floating-point and 12-bit fixed-point precision on the SAU and the plane wave systems, respectively. The iterative method with double precision floating-point coincides with the minimum RMS curve, and fixed-point approximation increases the RMS error slightly. Thus the iterative calculation method helps reduce the storage requirement significantly with almost no increase in RMS phase error.

4 The Evolution of Sonic Millip3De For Separable 2-D Array Beamforming

Recently, we proposed Sonic Millip3De [14], a front-end ultrasound system that combines algorithmic modification with numerous architectural techniques to achieve massive parallelism within a tight power budget. The Sonic

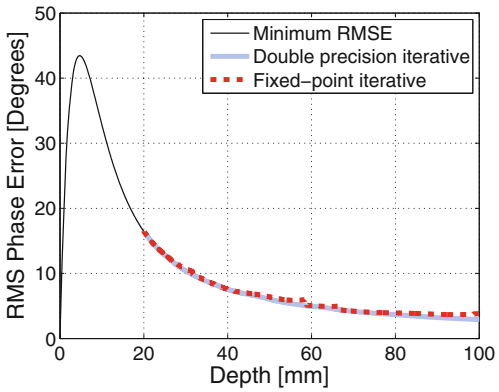

Figure 8 RMS phase error of SAU system.

Millip3De system is split among three distinct dies using an emerging IC fabrication technique that integrates several IC die layers on top of one another, such that wiring latency and power consumption are greatly reduced [1]. Figure 10 depicts the 3-layered architecture, wherein layers are stacked vertically and connected with through silicon vias (TSVs).

The first layer consists of a 120 × 88 grid of capacitive micromachined ultrasonic transducers (CMUTs) as well as other analog components. The received echo signals are sent to the second layer where 12-bit ADCs digitize the echos and store the signal in SRAM arrays. Finally, the third layer streams the data from the SRAMs, performing the entire delay-sum beamforming operation using multiple independent pipelines, and then sums across the channels to generate a complete output frame.

The third die layer's beamforming pipelines are each divided into three stages. During the first stage, a linear interpolation is performed on all of the data as it streams from the SRAM, up-sampling the data by a factor of 4×. The output is then sent to the second stage, known as the "select" unit, which selects the sample nearest each focal point from the incoming data stream. To better exploit data locality, the "select" unit is divided into 16 sub-units, each sharing the same input stream, but generating different scanlines of the final image. The selection process is done using an iterative piece-wise quadratic estimation method discussed in detail in [14]. The final stage of the pipeline is a 1,024 node network that applies a channel specific apodization constant and sums across the channels.

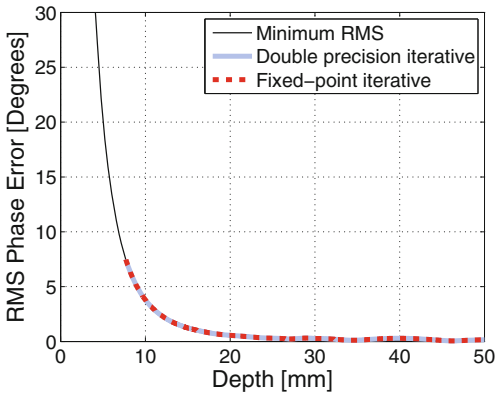

Figure 9 RMS phase error of plane wave system.

To facilitate separable beamforming, we replace the unidirectional ring network interconnecting the channels of the original design with a configurable mesh. The mesh allows both the original ring interconnection topology used for non-separable beamforming as well as smaller subnetworks required by first-stage beamforming in the separable schemes. For the separable configuration, we organize the accelerator and interconnect to form 32 independent 32-node clusters. In the first beamforming stage, scanline data is accumulated across the 32 nodes within a cluster. This data is then written back to SRAM, using the signal paths labeled "Stage 1" in Fig. 10b. Once the first beamforming stage is complete, the partially beamformed output is then passed through the accelerator a second time with constants for the second beamforming operation. In this stage, the network is reconfigured into the "Stage 2" paths shown in Fig. 10b, which run across the 32 clusters. Figure 11 shows the data flow within a cluster during the first stage (data flows from bottom to top) and across clusters during the second stage (data flows from left to right). After the second stage of beamforming is complete, the final output image is stored in off-chip DRAM. The additional reconfigurability of the system results in a small ($< 2\%$) power increase, but provides substantial flexibility ultrasound system.

Additionally, the support for separable beamforming greatly increases the throughput of the system. With 1,024 nodes and 16 sub-units per node, the separable configuration is able to process all 48 scanlines for the 1,024 transducer sub-aperture in Stage 1 in only 3 iterations. Stage 2 requires 6 iterations (due to the 1,536 channels of data produced by Stage 1) giving a total of 9 iterations per sub-aperture. This throughput increase is a 16× improvement over the 144 iterations required by the non-separable design. The system is also able to achieve additional power savings by power gating half of the channels in the last 3 iterations of stage 2 as only 512 channels remain to be processed, enabling an energy savings of nearly 19×.

The plane wave method described above differs significantly from SAU beamforming; however, Sonic Millip3De is able to support the algorithm with only minor additional hardware support. As described previously, in a separable plane wave system, each scanline is generated using echo data from only a small neighboring sub-set of channels, in contrast to the SAU system, where all channels contribute

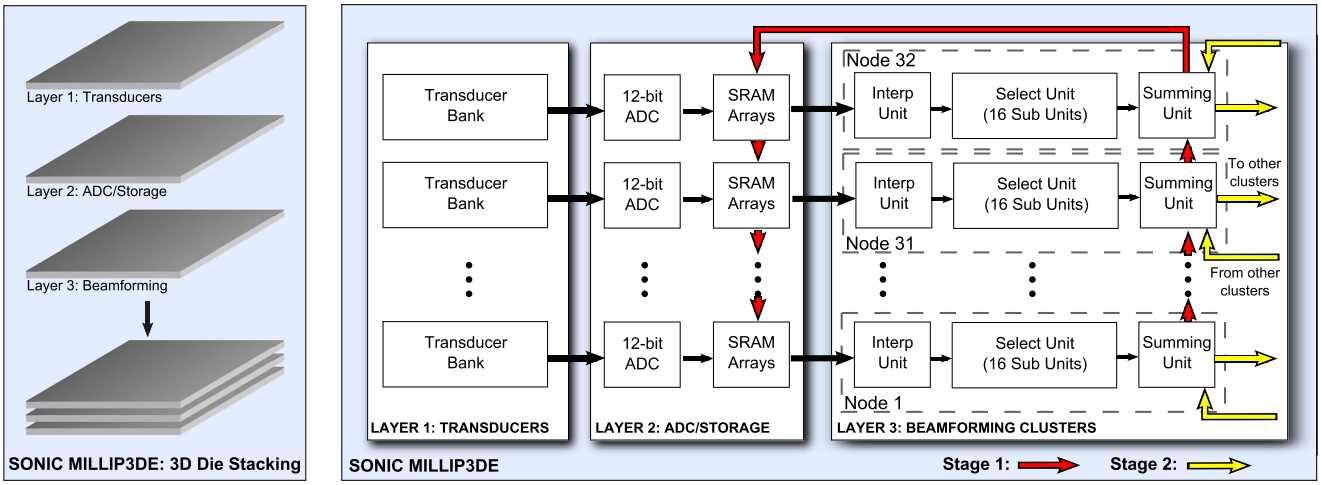

(a) 3 layer die stacking (b) Pipeline of a single 32 node cluster

Figure 10 Design of Sonic Millip3De for separable beamforming. Layer 3 contains 32 clusters with 32 nodes per cluster.

to every scanline. However, in the Sonic Millip3De system, each channel processes 16 scanlines independently and data that is not needed can easily be zeroed out using the apodization constant already supported in the hardware for data that does not correspond to the current scanline. Figure 12 shows a simple example where the 5th scanline uses data from channels 2, 3, and 4 (represented by their respective network nodes) and scanline 6 uses data from channels 3, 4 and 5. In the example, the image data processed in sub-unit of Node 5 for scanline 6 will have A3 as the apodization; however, the data generated by the sub-unit for scanline 5 will use 0 for apodization, and hence will not contribute to the beamforming. Overall the only additional hardware required to perform this operation is storage for 16 apodization constants (one per scanline processed) in each channel instead of the single constant required by SAU. The rest of the processing pipeline remains unchanged.

Despite the small changes to the hardware, the separable plane wave configuration greatly increases the peak frame rate of the beamforming accelerator. In a system with 32×32 scanlines, using 4 iterations per frame per beamforming stage, our hardware can produce up to 6,000 frames/second—over 100 times higher than our separable SAU system. This speedup does come at the cost of some image quality, but is promising for high-speed applications such as 3-D flow imaging and 3-D elastography where the image itself is not directly viewed and is instead used in non-visual processing. However, Sonic Millip3De is currently limited by available DRAM bandwidth and cannot output frames at the full rate they can be produced by the accelerator. Our future work will focus on integrating additional post-processing (e.g., for flow imaging) directly into the

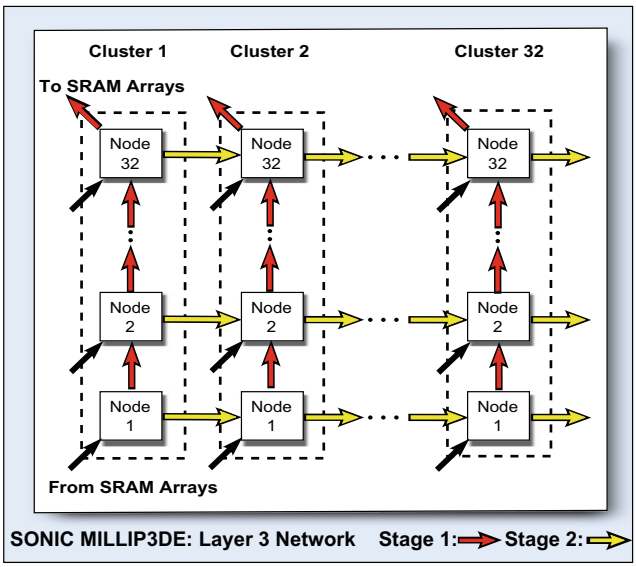

Figure 11 Data flow in stages 1 & 2 of beamforming for Layer 3: The processing units in a dashed box form a cluster; the black arrows correspond to data flow from SRAM arrays to nodes in a cluster. In the 1st beamforming stage the data flows from bottom to top, in the 2nd beamforming stage the data flows from left to right. The output data from the second beamforming stage is stored in the DRAM.

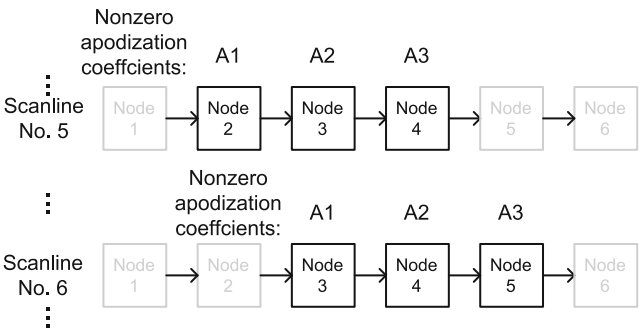

Figure 12 Dataflow diagram of plane wave separable beamforming.

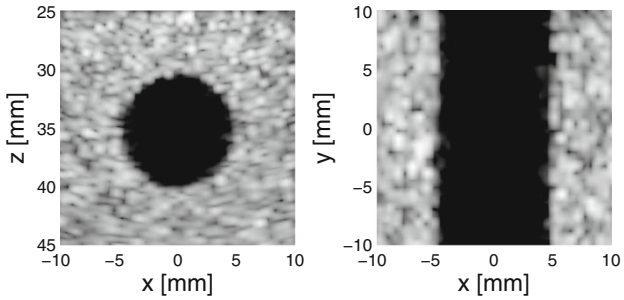

(a) Non-separable beamforming, double-precision-floating-point

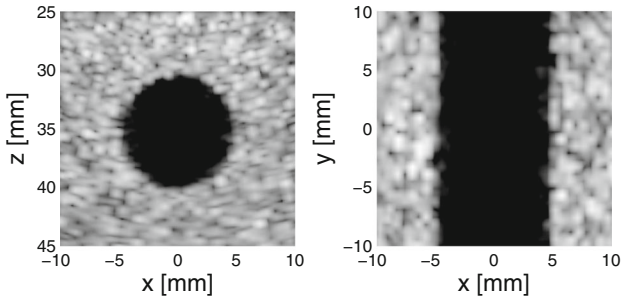

(b) Separable beamforming, double-precision-floating-point with iterative delay calculation

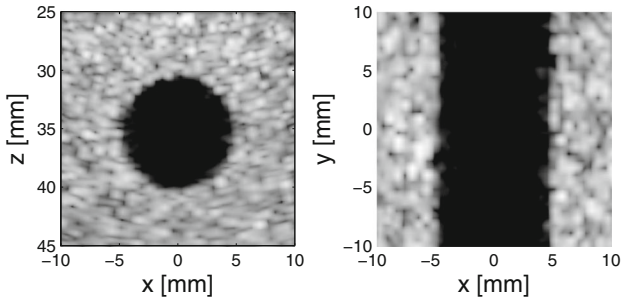

(c) Separable beamforming, 12-bit-fixed-point precision with iterative delay calculation

Figure 13 3-D slice images of SAU system, 40dB dynamic range.

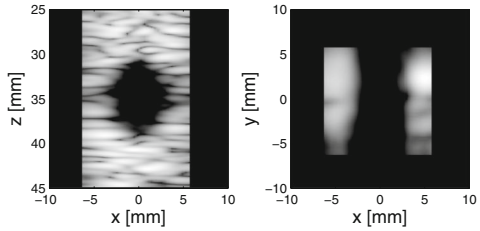

(a) Non-separable beamforming, double-precision-floating-point

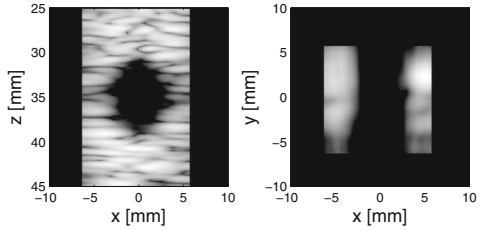

(b) Separable beamforming, double-precision-floating-point, algorithm in [13]

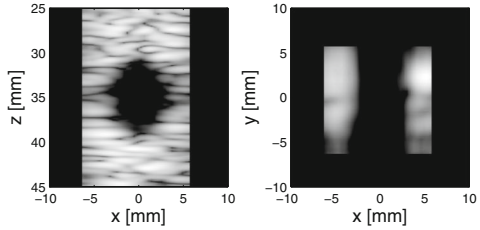

(c) Separable beamforming, double-precision-floating-point, minimum RMS delay decomposition

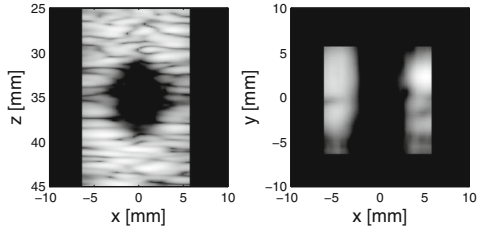

(d) Separable beamforming, 12-bit-fixed-point precision with iterative delay calculation

Figure 14 3-D slice images of plane wave system, 40dB dynamic range.

system, thus leveraging the high frame rate without communicating individual frames to memory through the limited DRAM interface.

5 Simulation Results

We use Field II [6, 8] and MATLAB simulation to verify the algorithm and the proposed system configuration. The SAU system configuration for depth ranging from 2cm to 10cm is shown in Table 1. For the plane wave system, the transducer array is the same as the SAU system, but the transducer spacing is a full wavelength, which is twice that of the SAU system. The receive aperture consists of 32×32 transducers, and the beamforming aperture consists of 20×20 transducers. The depth of the plane wave system is limited to 0.8cm to 5cm since its aperture is much smaller than the SAU system.

The simulation scenario is a 1cm wide cylindrical anechoic cyst placed at 3.5cm depth. The vertical and lateral slices of the 3-D volume generated with the SAU systems are shown in Fig. 13. The image quality obtained by the baseline non-separable beamforming and our proposed

separable beamforming method are nearly indistinguishable. Even the 12-bit-fixed-point beamforming and iterative delay calculation method can produce images with excellent quality. In all these three cases shown in Fig. 13 the contrast-to-noise ratio is 5.0. CNR is defined by Eq. 18:

$$\mathrm{CNR} = \frac{|\mu_{\mathrm{cyst}} - \mu_{\mathrm{bgnd}}|}{\sqrt{\sigma_{\mathrm{cyst}}^2 + \sigma_{\mathrm{bgnd}}^2}} \tag{18}$$

where μ_{cyst} and μ_{bgnd} correspond to the brightness of cyst and background, while σ_{cyst} and σ_{bgnd} are the standard deviation of cyst and background.

The simulation results of the plane wave system are shown in Fig. 14. All four cases achieve the same CNR value of 2.5. Note that our proposed delay decomposition with fixed-point beamforming and iterative delay calculation, which does not require multiplications and other complex operations other than additions/subtracts, can generate the 3-D image with the same quality as the non-separable method using double-floating-point precision data for calculation.

6 Conclusion

We presented a general separable beamforming method that decomposes 2-D array beamforming into two stages of 1-D array beamforming. Our approach is based on a delay decomposition method that minimizes phase error. The resulting method reduces the beamforming complexity of a SAU-based 3-D imaging system by 19×, and reduces the beamforming complexity of a plane-wave-based system by 12×, which can be used to increase frame rate in order to support applications requiring extremely high frame rate or decrease the power consumption for better battery life of handheld applications. Field II simulation results show that this method with fixed-point precision can generate images with high CNR that are comparable to those generated by the non-separable beamforming method running on double-floating-point precision. Finally, we present extensions to support separable beamforming for both SAU and plane wave systems on our recently proposed Sonic Millip3De. The extensions include changing the beamforming network from a pipelined ring into a mesh topology to support the new data flow pattern and adding additional SRAM buffers to store data between the two stages in a separable system.

Acknowledgments This work was partially supported by NSF CSR 0910699, CCF 1406739 and CCF 1406810. The authors thank the reviewers for their insightful comments and J. Brian Fowlkes, Oliver Kripfgans for many helpful discussions.

References

1. Black, B., Annavaram, M., Brekelbaum, N., DeVale, J., Jiang, L., Loh, G.H., McCaule, D., Morrow, P., Nelson, D.W., Pantuso, D., Reed, P., Rupley, J., Shankar, S., Shen, J., Webb, C. (2006). In *Die stacking (3D) microarchitecture*.
2. Campbell, S., Lees, C., Moscoso, G., Hall, P. (2005). Ultrasound antenatal diagnosis of cleft palate by a new technique: the 3D reverse face view. *Ultrasound in Obstetrics and Gynecology*, *25*(1), 12–18.
3. Choe, J.W., Oralkan, O., Khuri-Yakub, P. (2010). In *Design optimization for a 2-D sparse transducer array for 3-D ultrasound imaging. IEEE Ultrasonics Symposium (IUS) pp*: 1928–1931.
4. Dacorogna, B. (2004). In *Introduction to the Calculus of Variations*: World Scientific.
5. Dhanantwari, A.C., Stergiopoulos, S., Song, L., Parodi, C., Bertor, F., Pellegretti, P., Questa, A. (2004). In *An efficient 3D beamformer implementation for real-time 4D ultrasound systems deploying planar array probes*.
6. Jensen, J.A. (1996). FIELD: A program for simulating ultrasound systems. 10th Nordicbaltic Conference on Biomedical Imaging, Vol. 4, Supplement 1. *Part 1:351–353*, 351–353.
7. Jensen, J.A., Nikolov, S.I., GammelMark, K.L., Pedersen, M.H. (2006). Synthetic aperture ultrasound imaging. *Ultrasonics*, *44*(1), 5–15.
8. Jensen, J.A., & Svendsen, N.B. (1992). In *Calculation of pressure fields from arbitrarily shaped, apodized, and excited ultrasound transducers. IEEE Transactions on Ultrasonics Ferroelectrics and Frequency Control 39(2)*: 262 –267.
9. Karaman, M., Bilge, H.S., O'Donnell, M. (1998). In *Adaptive multi-element synthetic aperture imaging with motion and phase aberration correction. IEEE Transactions on Ultrasonics, Ferroelectrics and Frequency Control 45(4)*: 1077 –1087.
10. Karaman, M., Li, P.C., O'Donnell, M. (1995). Synthetic aperture imaging for small scale systems. *IEEE Transactions on Ultrasonics, Ferroelectrics and Frequency Control*, *42*(3), 429–442.
11. Karaman, M., Wygant, I.O., Oralkan, O., Khuri-Yakub, B.T. (2009). Minimally redundant 2-D array designs for 3-D medical ultrasound imaging. *IEEE Transactions on Medical Imaging*, *28*(7), 1051–1061.
12. Lockwood, G.R., Talman, J.R., Brunke, S.S. (1998). Real-time 3-D ultrasound imaging using sparse synthetic aperture beamforming. *IEEE Transactions on Ultrasonics, Ferroelectrics and Frequency Control*, *4*(4), 980–988.
13. Owen, K., Fuller, M.I., Hossack, J.A. (2012). Application of X-Y separable 2-D array beamforming for increased frame rate and energy efficiency in handheld devices. *IEEE Transactions on Ultrasonics, Ferroelectrics and Frequency Control*, *59*(7), 1332–1343.
14. Sampson, R., Yang, M., Wei, S., Chakrabarti, C., Wenisch, T.F. (2013). Sonic Millip3De: Massively parallel 3D stacked accelerator for 3D ultrasound. In: 19th IEEE International Symposium on High Performance Computer Architecture, pp. 318–329.
15. Sampson, R., Yang, M., Wei, S., Chakrabarti, C., Wenisch, T.F. (2013). Sonic millip3de with dynamic receive focusing and apodization optimization. In: Proceedings of IEEE International Ultrasonics Symposium, pp. 557–560.
16. Yagel, S., Cohen, S.M., Shapiro, I., Valsky, D.V. (2007). 3D and 4D ultrasound in fetal cardiac scanning: a new look at the fetal heart. *Ultrasound in Obstetrics and Gynecology*, *29*(1), 81–95.
17. Yang, M., Sampson, R., Wenisch, T.F., Chakrabarti, C. (2013). Separable beamforming for 3-D synthetic aperture ultrasound imaging. In: Proceedings of IEEE Workshop on Signal Processing Systems, pp. 207-212. Taipei, Taiwan.

Ming Yang is a PhD candidate in the School of Electrical, Computer and Energy Engineering at Arizona State University. His research focuses on the development of algorithms and low-power hardware for a handheld 3D ultrasound imaging device. Yang has an MS in electrical engineering from Beijing University of Posts and Telecommunications.

Richard Sampson is a PhD candidate in the Department of Computer Science and Engineering at the University of Michigan. His research interests include hardware system and accelerator design for imaging and computer vision applications. Sampson has a BA in Physics and a BS in Computer Engineering from Columbia University as well as an MS in Computer Science and Engineering from the University of Michigan.

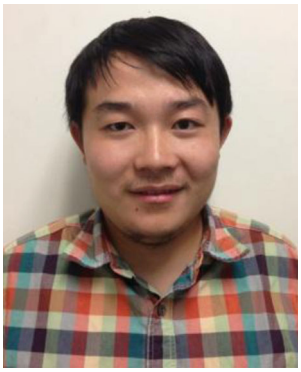

Siyuan Wei is a PhD student in the School of Electrical, Computer and Energy Engineering at Arizona State University. His research focuses on algorithm-architecture codesign of ultrasound imaging systems, especially those based on Doppler imaging. Wei has a BE in electrical engineering from Huazhong University of Technology and Science.

Thomas Wenisch is an Associate Professor of Electrical Engineering and Computer Science at the University of Michigan and a member of the Advanced Computer Architecture Lab (ACAL). His research interests center on computer architecture with particular emphasis on multiprocessor and multicore systems, smartphone architecture, data center architecture, 3D medical imaging applications, and performance evaluation methodology. Wenisch received his PhD from Carnegie Mellon University.

Chaitali Chakrabarti received the B.Tech. degree in electronics and electrical communication engineering from the Indian Institute of Technology, Kharagpur, India, in 1984, and the M.S. and Ph.D. degrees in electrical engineering from the University of Maryland, College Park, in 1986 and 1990, respectively. She is a Professor with the School of Electrical Computer and Energy Engineering, Arizona State University (ASU), Tempe, and a Fellow of the IEEE. Her research interests include the areas of low power embedded systems design, and VLSI architectures and algorithms for signal processing and communications. She is currently an Associate Editor of the Journal of VLSI Signal Processing Systems, the IEEE Transactions of VLSI Systems and on the Senior Editorial Board of IEEE Journal on Emerging and Selected Topics in Circuits and Systems.